Role of ceramic matrix and Au fraction on the morphology and optical properties of cosputtered Au-ceramic thin films

S. Hazra[a)]
Surface Physics Division, Saha Institute of Nuclear Physics, 1/AF Bidhannagar, Kolkata 700 064, India

A. Gibaud
Laboratoire de Physique de l'Etat Condensé, Faculté des Sciences, Université du Maine, 72085 Le Mans, France

C. Sella
Laboratoire d'Optique des Solides, Université de Paris VI, 75252 Paris, France

(Received 21 February 2007; accepted 18 April 2007; published online 13 June 2007)

Surface sensitive x-ray scattering studies were carried out to understand the morphology of cermet thin films prepared by cosputtering metallic gold and ceramic materials on float glass substrates. It has been observed that the morphology of Au clusters in cermet thin films depends strongly on the matrix during growth, even if, all other conditions are kept identical. In particular, nearly isotropic growth of Au clusters, to form nanoparticles, is found in silica and alumina matrices, while anisotropic columnar-like growth of Au clusters, to form a nanorod-like shape, is found in a titanium oxide matrix. Thickness of the films was also found very different, which is likely to be related to the different sputtering yields of the ceramic materials. The volume fraction of Au estimated from the electron density profile shows that the total volume or the amount of Au is different in films of different ceramic matrices. This suggests that even the sputtering yield of Au is very different in the presence of different ceramic atmosphere, which is likely to be responsible for having a different morphology of Au clusters in different matrices. Optical absorption spectra of the films, on the other hand, show linear dependence of the absorption peak position with the volume fraction of Au and independent of both the ceramic matrix and morphology of Au clusters. © *2007 American Institute of Physics*. [DOI: 10.1063/1.2745124]

I. INTRODUCTION

Ceramic thin films containing Au clusters are found to be interesting composite materials for optical[1] and other applications.[2] These nanocomposites or nanocermets exhibit large absorption near ultraviolet visible (UV-VIS) region[3–8] when Au is present as confined materials, such as in the form of nanoparticles, nanorods, etc. Optical properties of these nanocermet films are thought to be related to the shape, size, and distribution of the Au clusters in the films[7] apart from the ceramic matrix itself, which in turn can strongly vary with the ceramic matrix and the concentration of Au present during growth. It is thus important to determine the role of the ceramic matrix and volume fraction of Au in the morphology of nanocermet films and to compare that with the optical properties.

The morphology of a film can be studied using surface sensitive x-ray scattering techniques in nondestructive and statistical ways.[7,9–11] Specular reflectivity provides the structure of the film along the growth direction,[7,9–12] i.e., it can provide film thickness and in-plane $(x-y)$ average electron density as a function of depth (z). From the electron density it is possible to extract volume fraction of the metal in cermet film. On the other hand, recently developed grazing incidence small angle scattering (GISAXS) provides average size, shape, and distribution of clusters in the matrix[13,14] or in the substrate.[15–17] Combination of reflectivity and GISAXS can bring out the morphological information[7,11,18–20] along with the volume fraction of Au in the system. In this article we will present the morphology and optical properties of Au-ceramic thin films and from the analysis it will be elucidated that the sputtering conditions and thus the morphology of the films changes strongly with ceramic material present during growth, while the optical properties solely depend on the volume fraction of Au in the cermet films.

II. EXPERIMENTS

Cermet thin films (indicated in Table I) were made by sputtering Au-ceramic disks on float glass substrates. Three films labeled as AT07, AT19, and AT38 were prepared from three Au-TiO_2 disks having 7, 19, and 38 numbers of small Au pellets on big TiO_2 disk, respectively, to get films having a different volume fraction (f) of Au. To see the matrix effect, two additional films, labeled as AA42 and AS42, were prepared from Au-Al_2O_3 and Au-SiO_2 disks having 42 numbers of small Au pellets on big Al_2O_3 and SiO_2 disks, respectively, under similar deposition condition and time, that of AT38.

X-ray reflectivity of the films were performed using a laboratory source x-ray scattering setup of the wavelength 1.54 Å. GISAXS measurements of the films were performed using synchrotron source (D22 beam line, LURE) at energy 7 keV and the reciprocal space maps were collected using a

[a)]Electronic mail: satyajit.hazra@saha.ac.in

TABLE I. Parameters of the Au-ceramic thin films obtained from the analysis of the x-ray scattering measurements.

Sample	Label	t (nm)	f	σ_{top} (nm)	$2R_{xy}(\sigma_R)$ (nm)	$2R_z(\sigma_R)$ (nm)	$d_{xy}(\sigma_d)$ (nm)	$d_z(\sigma_d)$ (nm)	d_L (nm)	λ_p (Å)
7Au-TiO_2	AT07	69	0.16	3.2	2.6 (0.2)[a]		3.7 (0.8)[a]			557
19Au-TiO_2	AT19	87	0.31	3.7	2.9 (0.2)[a]		3.9 (0.9)[a]			602
38Au-TiO_2	AT38	60	0.49	4.5	3.2 (0.2)[a]		4.0 (0.9)[a]			656
42Au-Al_2O_3	AA42	74	0.17	4.0	4.6 (0.5)	4.8 (0.6)	5.4 (1.4)	6.2 (1.4)	6.5	566
42Au-SiO_2	AS42	140	0.18	4.2	3.2 (0.2)	4.0 (0.5)	4.1 (0.9)	4.7 (1.0)	4.9	

[a]Estimation is not very accurate.

two-dimensional (2D) detector (see Ref. 11 for details). An inverted T-type mask has been used in front of the detector to avoid saturation from the direct and the specularly reflected beams. Optical absorption spectra of the films were collected using an UV-VIS spectrophotometer (Cintra 10e, GBC).

III. RESULTS AND DISCUSSION

A. Morphological studies

Reciprocal space maps of the Au-TiO_2 films obtained from GISAXS measurements are shown in Fig. 1. All the images show the presence of an intense region close to the center, which is faint for the AT07 film. The intensity close to the center corresponds to the scattering near the critical angle of the total external reflection convoluted with the surface roughness. For AT07 film, faint diffuse spots along q_y on both sides of $q_z=0$ are visible. The presence of these spots is due to an average in-plane separation between Au clusters. These spots merge to the central spots as we move to films AT19 and AT38. This is due to the increase in Au-clusters separation, which is associated with the increase in size of Au clusters with a volume fraction of Au. The absence of an annular ring or spots along q_z indicates that along the z direction, either there are no regular size and separation in the clusters or those are quite large in these films.

The GISAXS images of three Au-cermet films for different ceramic matrices are shown in Fig. 2 for comparison. It can be noted that nearly symmetric annular rings are present in both AS42 and AA42 films, unlike that in AT38 film. The shape of the ring is related to the shape, size, and distribution of the particles in the films. The distance of the ring from the origin is related to the average separation of the cluster particles in a particular direction. The nearly symmetric annular rings in AS42 and AA42 films indicate the presence of Au nanoparticles in SiO_2 and Al_2O_3 matrices, while the presence of the side diffuse spots in the AT38 film is the signature of columnar-like growth of an Au cluster in the TiO_2 matrix, which are like nanorods (i.e., nanoparticles extended in the z direction compared to that of the $x-y$ plane).

The x-ray reflectivity data of three Au-TiO_2 films are shown in Fig. 3. All the reflectivity curves follow the similar behavior, namely, high reflectivity due to total external reflection, rounding of the reflectivity curve due to the high absorption, followed by a sharp decrease due to the surface roughness and Kiessig fringes due to the total film thickness.

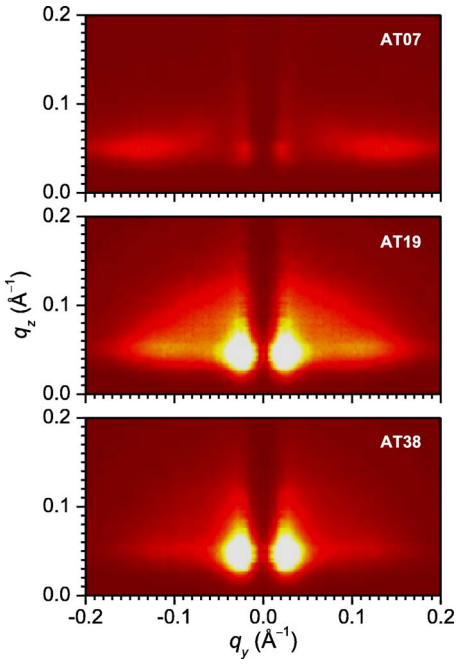

FIG. 1. (Color online) 2D GISAXS intensity for three Au-TiO_2 cermet thin films of different volume fractions of Au, collected at a fixed incidence angle.

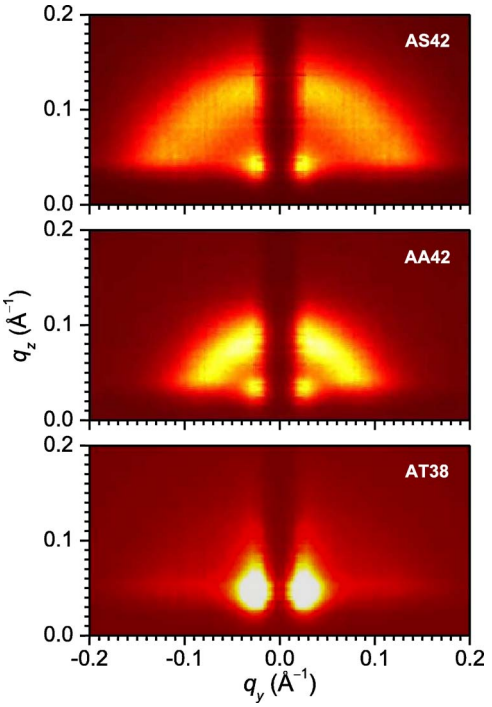

FIG. 2. (Color online) 2D GISAXS intensity for three Au-ceramic thin films of different ceramic matrices, collected at a fixed incidence angle.

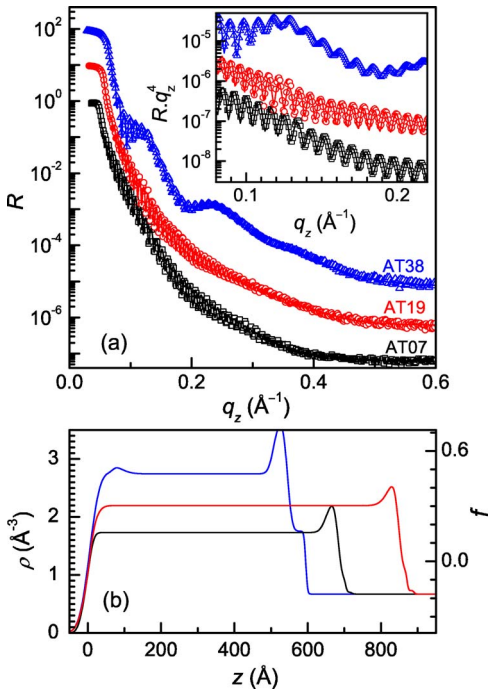

FIG. 3. (Color online) (a) Reflectivity data (symbols) of the three Au-TiO_2 cermet thin films of different concentration of Au. Inset: Enlarged view of selected portion of the reflectivity curves multiplied by q_z^4 to show the Kiessig fringes due to the total film thickness. Solid lines passing through the reflectivity data are the best fit curves. Curves have been shifted vertically for clarity. (b) Corresponding EDP along with the volume fraction of Au in the film.

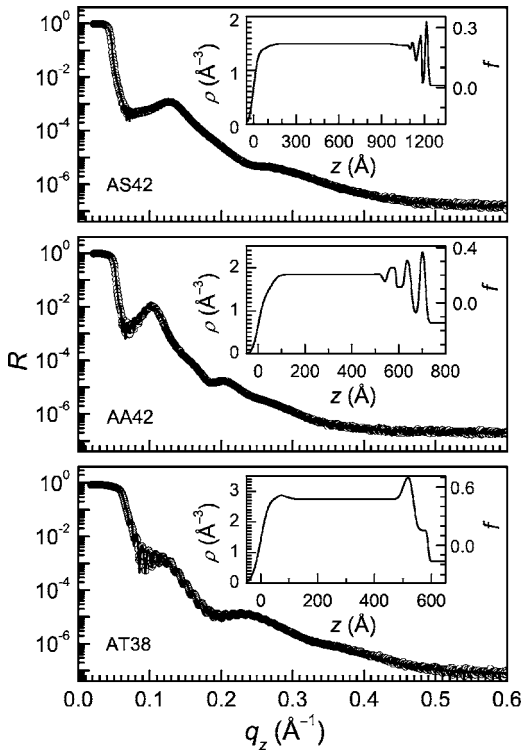

FIG. 4. Reflectivity data (symbols) of the three Au-ceramic thin films of different ceramic matrices are in three different panels. Solid lines passing through the reflectivity data are the best fit curves. The inset of each panel shows the corresponding EDP along with the volume fraction of Au in the film.

A broad hump is observed in the AT38 film, which is absent in the other two films. The presence of Kiessig fringes in all three films and the broad hump in AT38 film only are very prominent in the enlarged view of the selected portion as shown in the inset of Fig. 3.

The x-ray reflectivity data of three Au-cermet films of different ceramic matrices are shown in Fig. 4. The reflectivity curves are similar to those of Fig. 3. The only difference is that the broad hump is present in all the films. The position of the broad hump, which is related to a separation (d_L) along the z direction, here presumably between two high density Au-regions, is, however, varied for different films.

As observed in Figs. 3 and 4, the position of the rounding, which is related to the average critical wave vector (q_c), and the separation between the Kiessig fringes, which is related to the total film thickness (t), is different in different films. The average critical wave vector is again related to the average electron density (ρ) of the film and from that one can extract f of Au in the film applying simple relation

$$x = \frac{\rho_{\text{film}} - \rho_{\text{matrix}}}{\rho_{\text{Au}} - \rho_{\text{matrix}}} = \frac{q_{c,\,\text{film}}^2 - q_{c,\,\text{matrix}}^2}{q_{c,\,\text{Au}}^2 - q_{c,\,\text{matrix}}^2}. \tag{1}$$

Using the value of q_c for Au as 0.079 Å^{-1} and that for the TiO_2, Al_2O_3, and SiO_2 matrix materials as 0.042, 0.041, and 0.031 Å^{-1}, respectively, the value of f has been estimated from Eq. (1) and listed in Table I for all the films. Table I shows that f increases gradually for AT07, AT19, and AT38 films but remains almost the same for AA42 and AS42 films, which is much less compared to that in AT38 film.

To extract the details quantitative morphological information of the films, the x-ray scattering data have been analyzed considering the electron density of a thin film, in which metal clusters are randomly distributed in the amorphous matrix. The electron density for such a heterogeneous thin film can be written as[11]

$$\rho(r) = \left[\rho_{\text{matrix}} + \Delta\rho \sum_i \delta(r - r_i) \otimes S_c(r_i)\right] S_F(r), \tag{2}$$

where $\Delta\rho = \rho_{\text{Au}} - \rho_{\text{matrix}}$, $\delta(r - r_i)$ is related to the distribution of the clusters, $S_c(r_i)$ is related to the shape and size of the ith cluster at a position r_i, and $S_F(r)$ is related to the finite dimension of the film. In the intensity calculation, we can assume that the part of the incident beam is reflected by the film interfaces and the part of it is scattered by the cluster (which have different electron densities compared to the matrix) grains. Then in a kinematical approximation the total scattered intensity (I) can be written as the sum of two intensities arising separately from the matrix (I_m) and the clusters (I_c) (neglecting the matrix-clusters crossterm) as

$$I(q) = I_m(q) + I_c(q). \tag{3}$$

It can be noted that the contribution of I_m is arising from the matrix of the uniform electron density, which is extended in the $x-y$ plane but confined in the z direction. This indicates that the variation in I_m is expected only along the z direction, while a nearly similar variation in I_c is expected in all directions. Considering the earlier argument, the total intensity can be written as

$$I(q) = R(q_z) + I_s(q), \tag{4}$$

where $R(q_z)$ is the intensity along the specular direction and $I_s(q)$ is that other than specular direction.

Calculation of $R(q_z)$ has been made considering it as reflectivity and for that each film of thickness t has been divided into a number of slices of different electron density and used matrix formalism.[12] It can be noted that, although we have started with the kinematical approach in calculating total intensity, the reflectivity calculation is quite complete, that is refraction as well as multiple scattering effects have been taken into account. The reflectivity data thus fitted are shown in Figs. 3 and 4 along with the electron density profile (EDP). For the Au-TiO_2 system, high electron density close to the substrate, which can be attributed to the segregation of Au clusters followed by a nearly uniform electron density, is observed. While for AS42 and AA42 films, oscillations close to the substrate are observed, which die-out along the film thickness and can be attributed to the cumulative distribution of Au clusters starting from the substrate. Different parameters obtained from the EDPs are listed in the Table I. It can be noted that although the growth parameters for AT38, AA42, and AS42 films are nearly same, the film thickness differs considerably. This is primarily due to the different sputtering yield (γ) of ceramic materials. Results suggest that $\gamma_{SiO_2} > \gamma_{Al_2O_3} > \gamma_{TiO_2}$. Also the value of f obtained from the EDP and/or q_c for films of different ceramic matrices suggest that $\gamma_{Au(TiO_2)} > \gamma_{Au(SiO_2)} > \gamma_{Au(Al_2O_3)}$, that is the sputtering yield of Au is even different in presence of different ceramic environment.

$I_s(q)$ in Eq. (4) is essentially the small angle scattering term arising from clusters and can be calculated in the following way:[18,21,22]

$$I_s = AQP + I_B, \tag{5}$$

where A is a constant related to the number and relative density of clusters, Q is a form factor arising from the average shape and size of clusters, P is a structure factor related to the clusters distribution, and I_B is the background effect. If we consider clusters to be spherical particles of radius R, distributed in the matrix according to a cumulative disorder with average separation d, then

$$Q = \frac{[\sin(qR) - qR\cos(qR)]^2}{(qR)^6}, \tag{6}$$

where the size of the clusters is assumed to follow Gaussian distribution with variance σ_R. On the other hand, if we consider the clusters to be full spheroid-like particles (as discussed in the manual of InGISAXS software[17]) then the functional form of Q will be slightly different. Even for that, in a particular direction it can be approximated to Eq. (6), without much error considering that the asymmetry, if any, will appear as different values of R in different directions. The structure factor, on the other hand, can be calculated using

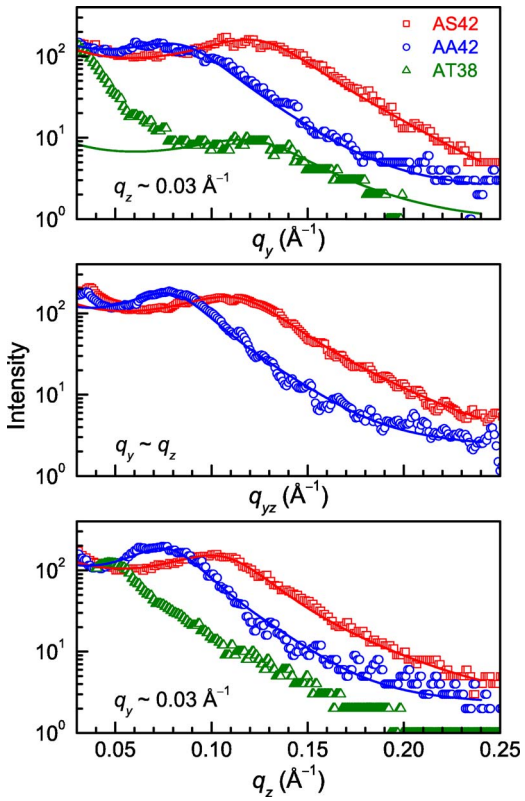

FIG. 5. (Color online) Line profiles (symbols) have drawn through GISAXS images along different directions for three Au-ceramic thin films of different ceramic matrices. Solid lines corresponding to the data are the calculated line profiles.

$$P = \frac{1 - \exp(-2q^2\sigma_d^2)}{1 - 2\cos(qd)\exp(-q^2\sigma_d^2) + \exp(-2q^2\sigma_d^2)}, \tag{7}$$

where σ_d is the variance of d. It can be noted that for three-dimensional disordered arrays, the dominating terms are the distance between a pair of particles and the number of such pairs in a given direction. Using this concept, it can be approximated with the one-dimensional paracrystal model [which gives rise Eq. (7)], where σ_d should be fairly high, such that the first nearest neighbor is only dominating and the number of scatterers in a particular direction (appearing from the pair) is quite small (the effect will go into term A). In actual calculation one has to take into account the effect of the reduced dimension of the film. The analysis of the GISAXS data has been made by drawing line profiles through the images along different directions. Using Eqs. (5)–(7), the particle size and the interparticle separation have been calculated. The value of the parameters obtained are listed in the Table I, while the experimental data and the calculated line profiles for three Au-cermet films of different matrices are shown in Fig. 5. It can be noted that the calculation of I_s is based on a kinematical approach and it does not include the effect of the Yoneda wings. However, using this simple approach the basic result should not differ much. The effect of the Yoneda wing is expected to arise along q_z scans. For AS42 and AA42 samples, the peak that is observed is a part of an annular ring and the position is far from the Yoneda wing (the position of the Yoneda wing should be around the value of q_c, which is ≤ 0.05 Å^{-1}, as is evident

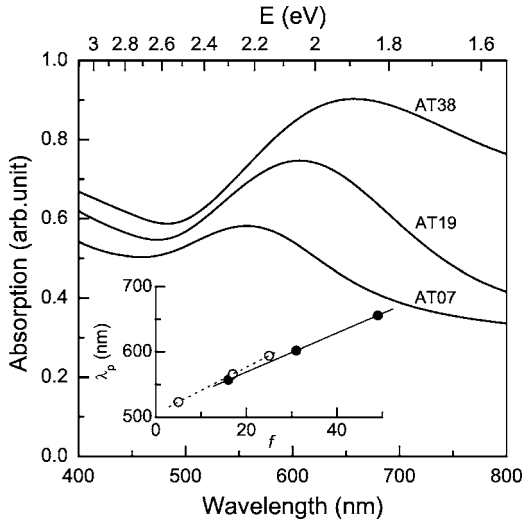

FIG. 6. Optical absorption spectra of Au-TiO_2 nanocermet films with three different volume fractions of (f) of Au. The inset shows a variation of the absorption peak position (λ_p) as a function of f for both Au-TiO_2 (solid symbols) and Au-Al_2O_3 (open symbols) systems. Solid and dashed straight lines are through the data of the two systems, respectively.

from reflectivity measurements). If both the positions are close, then due to the presence of the Yoneda wing, the peak position in the experimental curve may have a possibility to shift slightly toward a lower q_z value (which is otherwise at a slightly higher value). It is necessary to mention that the size of the particles listed in Table I for the Au-TiO_2 system is along the $x-y$ plane only and the estimation is not very accurate. Also the GISAXS image of such a system does not allow us to estimate the parameters along the z direction, quantitatively. However, qualitatively it can be understood that the value of the parameters is quite high and less regular. On the other hand, the size and distribution of Au particles in the AA42 and AS42 films are nearly symmetric (slightly elongated in the z direction) and regular. One of the reasons for such a difference in the morphology of the Au-TiO_2 system compared to that of the Au-Al_2O_3 and Au-SiO_2 systems may be due to the different sputtering yields as discussed before.

B. Optical absorption

Optical absorption spectra of three Au-TiO_2 films are shown in Fig. 6. A strong absorption peak is observed in all the films, which can be attributed to the surface plasmon resonance[1,4,5,7] of small Au clusters in the TiO_2 matrix. The value of the absorption peak position (λ_p) is listed in Table I, which suggests that λ_p shifts toward a higher wavelength with the increase of f of Au in the films. To understand the dependence, λ_p has been plotted as a function of f in the inset of Fig. 6. For comparison, data of Au-Al_2O_3 films[7] are also included in the same inset. It can be noted that λ_p shows linear dependence with f similar to that observed for Au-Al_2O_3 films, although the morphology of the two systems is quite different. The data of two different systems can even be fitted with a single straight line as is evident from the inset of Fig. 6. This suggests that although the shape of the Au clusters in the TiO_2 matrix is asymmetric (elongated along the z direction), the aspect ration is not high enough to give rise to different optical properties usually observed for nanorods[23,24] (namely, appearance of both transverse and longitudinal modes). It is interesting as this verifies the morphology of the system as predicted by the x-ray scattering measurements and indicates that the optical properties of such a nanocomposite system can be tuned solely through the volume fraction of Au.

IV. CONCLUSION

Morphology of Au-ceramic thin films deposited by radio frequency sputtering on float glasses has been studied by x-ray scattering techniques to understand the effect of ceramic materials on the growth of cermet films. The film thickness and volume fraction of Au estimated from the analysis of x-ray reflectivity data clearly suggest that the sputtering yield of different ceramic materials and also the sputtering yield of Au in the presence of different ceramic matrices are different. Analysis of GISAXS data suggests that in Au-SiO_2 and Au-Al_2O_3 cermet films, Au clusters form nanoparticles and are distributed in the ceramic matrices in a cumulative disorder starting from the substrate, while in the Au-TiO_2 film, Au clusters are extended in the growth direction to form a nanorod-like shape, with some segregation close to the substrate. Such a change in the morphology of Au clusters from nearly symmetric nanoparticles to asymmetric nanorod-like particles in cermet films for switching the ceramic matrix from silica or alumina to titanium oxide during film growth is likely to be related strongly to the relative sputtering yield of Au in a ceramic environment. The optical properties of the cermet films are, however, independent of the morphology and the optical absorption wavelength is only related linearly to the volume fraction of Au in the film.

ACKNOWLEDGMENTS

The authors are greatly indebted to the LURE facility for the GISAXS measurements, particularly to O. Lyon and A. Naudon.

[1] C. Flytzanis, F. Hache, M. C. Klein, D. Ricard, and P. Roussingnol, Prog. Opt. **XXIX**, 323 (1991).
[2] M. Valden, X. Lai, and D. W. Goodman, Science **281**, 1647 (1998).
[3] G. A. Niklasson and C. G. Granqvist, J. Appl. Phys. **55**, 3382 (1984).
[4] W. P. Halperin, Rev. Mod. Phys. **58**, 533 (1986).
[5] S. Link and M. A. El-Sayed, J. Phys. Chem. B **103**, 8410 (1999).
[6] Z. S. Li, C. X. Kan, and W. P. Cai, Appl. Phys. Lett. **82**, 1392 (2003).
[7] S. Hazra, A. Gibaud, and C. Sella, Appl. Phys. Lett. **85**, 395 (2004).
[8] E. György, G. Sauthier, A. Figueras, A. Giannoudakos, M. Kompitsas, and I. N. Mihailescu, J. Appl. Phys. **100**, 114302 (2006).
[9] I. K. Robinson and D. J. Tweet, Rep. Prog. Phys. **55**, 599 (1992).
[10] *X-Ray and Neutron Reflectivity: Principles and Applications*, edited by J. Daillant and A. Gibaud (Springer, Paris, 1999).
[11] S. Hazra, A. Gibaud, A. Desert, C. Sella, and A. Naudon, Physica B (Amsterdam) **283**, 97 (2000).
[12] A. Gibaud and S. Hazra, Curr. Sci. **78**, 1467 (2000).
[13] A. Naudon and D. Babonneau, Z. Metallkd. Z. Metallkd. **88**, 596 (1997).
[14] A. J. Allen, J. Am. Ceram. Soc. **88**, 1367 (2005).
[15] J. H. Li, V. Holy, M. Meduna, S. C. Moss, A. G. Norman, A. Mascarenhas, and J. L. Reno, Phys. Rev. B **66**, 115312 (2002).
[16] A. Barbier, S. Stanescu, C. Boeglin, and J.-P. Deville, Phys. Rev. B **68**, 245418 (2003).

[17]C. Revenant, F. Leroy, R. Lazzari, G. Renaud, and C. R. Henry, Phys. Rev. B **69**, 035411 (2004); R. Lazzari, Manual of InGISAXS software, http://www.insp.jussieu.fr.
[18]M. Rauscher, T. Salditt, and H. Spohn, Phys. Rev. B **52**, 16855 (1995).
[19]A. Gibaud, S. Hazra, C. Sella, P. Laffez, A. Désert, A. Naudon, and G. Van Tendeloo, Phys. Rev. B **63**, 193407 (2001).
[20]A. Gibaud, A. Baptite, D. A. Doshi, C. J. Brinker, L. Yang, and B. Ocko, Europhys. Lett. **63**, 833 (2003).
[21]A. Guinier and G. Fournet, *Small-Angle Scattering of X-Ray* (Wiley, New York, 1955).
[22]B. K. Vainshtein, *Diffraction of X-Rays by Chain Molecules* (Elsevier, Amsterdam, 1966).
[23]S. Link, M. B. Mohamed, and M. A. El-Sayed, J. Phys. Chem. B **103**, 3073 (1999).
[24]N. Felidj, J. Aubard, G. Levi, J. R. Krenn, G. Schider, A. Leitner, and F. R. Aussenegg, Phys. Rev. B **66**, 245407 (2002).